nature physics

Article

https://doi.org/10.1038/s41567-023-02115-2

Demonstration of momentum cooling to enhance the potential of cancer treatment with proton therapy

Received: 23 August 2022

Accepted: 26 May 2023

Published online: 3 July 2023

Check for updates

Vivek Maradia[1,2] ✉, David Meer[1], Rudolf Dölling[1], Damien C. Weber[1,3,4], Antony J. Lomax[1,2] & Serena Psoroulas[1]

In recent years, there has been a considerable push towards ultrahigh dose rates in proton therapy to effectively utilize motion mitigation strategies and potentially increase the sparing of healthy tissue through the so-called FLASH effect. However, in cyclotron-based proton therapy facilities, it is difficult to reach ultrahigh dose rates for low-energy beams. The main reason for this lies in the large momentum spread that such beams have after reducing their energy to levels required for proton therapy, incurring large losses in conventionally used momentum or energy selection slits. Here we propose momentum cooling by using a wedge in the energy selection system (instead of a slit) to reduce the momentum spread of the beam without introducing substantial beam losses. We demonstrate this concept in our eye treatment beamline and obtain a factor of two higher transmission, which could eventually halve the treatment delivery time. Furthermore, we show that with a gantry design incorporating this feature, we can achieve almost a factor of 100 higher transmission for a 70 MeV beam compared with conventional cyclotron-based facilities. This concept could enhance the potential of proton therapy by opening up possibilities of treating new indications and reducing the cost.

Ninety-two years since the invention of the cyclotron by E. Lawrence, over 1,500 cyclotron facilities, operating in 95 countries around the world, produce high-energy proton beams for radioisotope production, cancer treatments and multidisciplinary research[1]. Over the last ten years, the number of cyclotron-based proton therapy (PT) facilities has increased exponentially[2], as PT provides improved dose conformity and healthy tissue sparing compared with equivalent conventional radiation (photon/electron) therapy plans[3–5]. Cyclotrons are currently the most common accelerators for PT, accounting for two-thirds of the total installations.

Since a cyclotron produces beams of fixed energy (230–250 MeV for a PT cyclotron), to achieve clinically required energies (70–230 MeV), an energy selection system (ESS), consisting of a degrader of adjustable thickness, is required. Multiple Coulomb scattering and range straggling in the degrader increase the transverse emittance (phase-space area) and the momentum/energy spread of the beam beyond the acceptance of the following beamline[6,7], resulting in an energy-dependent beam transmission. For most facilities, and for the lowest energies (70–100 MeV), transmission through the ESS is typically below 0.1% (refs. 6,8). Such losses cause an undesirable increase in treatment delivery time, particularly when combined with motion mitigation techniques[9] (~15–30 min for a field delivery), and reduce patient comfort. Indeed, there is growing interest in the radiotherapy community to reduce treatment times through increased dose rates, both for biological reasons (exploiting the so-called FLASH irradiations[10]) and to help mitigate these effects of internal organ motions during therapy[11].

[1]Paul Scherrer Institute, Würenlingen, Switzerland. [2]ETH Zurich, Zurich, Switzerland. [3]University Hospital Zurich, Zurich, Switzerland. [4]University Hospital Bern, University of Bern, Bern, Switzerland. ✉e-mail: vivek.maradia@psi.ch

Matching the momentum spread of the beam after energy degradation, through the use of momentum selection slits, substantially contributes to this transmission loss through the ESS[8]. Despite efforts to achieve efficient PT treatment delivery, no single method has emerged as a viable, generally applicable alternative solution in terms of transmission improvement from the cyclotron to the treatment location (also called the isocentre).

As such, here we propose a method called 'momentum cooling' to reduce longitudinal emittance (momentum spread) after energy degradation, a technique previously proposed for muon ionization cooling experiments[12–14]. To the best of our knowledge, this technique has never been proposed to improve transmission in PT, perhaps due to the fact that it increases the transverse emittance of the beam, which is typically already relatively high in therapeutic proton beams (>100 π mm mrad (2σ value)).

However, in previous studies, we have already shown that such high emittances can be successfully controlled in PT beamlines. For instance, an asymmetric collimator can optimally match the beam emittance and the beamline acceptance to maximize transmission[8], whereas beam-optics imaging factors (equal to the ratio of beam size between the start point and end point) of the order of 2:1 or 3:1 between the entrance of the gantry and the isocentre can also let higher emittances through the gantry and thus improve the total transmission from the cyclotron to isocentre[15,16]. By combining these two techniques, we have demonstrated that it is possible to increase transmission for low-energy beams by a factor of 6 from 0.13% to 0.72% (ref. 8). Such improvements, however, are still limited by the losses due to energy selection. Changes in degrader material also can give only limited improvements to the transmission. To overcome this problem and maximizing the transport efficiency of high emittances, we propose to combine these methods with momentum cooling for a dramatic improvement in transmission.

In this Article, we present the experimental demonstration of wedge-based momentum cooling to achieve high transmission (high dose rates) for low-energy beams in a clinical proton beamline. We also propose a compact gantry design that includes momentum cooling capabilities and estimates the achievable transmissions and dose rates using Monte Carlo simulations.

Limitation of conventional state-of-the-art ESS

The schematic of a conventional ESS is shown in Fig. 1. At the entrance of dipole magnet D1, the source of the proton beam has a momentum of $p \pm \Delta p$. When the beam passes through D1, higher-momentum particles (that is, $p + \Delta p$) will bend less, while lower-momentum particles (that is, $p - \Delta p$) will bend more. A pair of focusing magnets (Q1 and Q2) are used to focus the beam at the momentum selection slit. By adjusting the position of the slit in the bending plane, one can, therefore, select different momentum bands. To achieve a Bragg peak with a sharp distal penumbra, a necessity for sparing normal tissues in PT, it is important to have momentum spreads as small as ±0.25%, particularly when treating small ocular targets using low-energy proton beams[17]. However, after the energy degrader, the momentum spread of the beam is in the range of ±4% for low energies, which introduces a substantial beam loss in the slits, resulting in a 6–10 times decrease in beam intensity[6,8,18].

The new ESS with momentum cooling

We propose to use a wedge instead of slits in the ESS to cool momentum spread without introducing a substantial loss of particles. Figure 2 illustrates the principle of the new ESS. The geometry of the wedge is chosen in a way that particles with different momenta will see different thicknesses of the material, thereby losing more (higher-energy particles) or less (lower-energy particles) energy in the wedge to equalize the momentum spread ($p - \Delta p$) after the wedge. Momentum spread after the wedge is, thus, reduced without introducing substantial beam losses, but at the cost of an increased emittance in the bending plane.

Demonstration of momentum cooling in clinical PT beamline

The OPTIS2 beamline at our institute has been designed and implemented specifically for the treatment of ocular tumours. For this, a carbon degrader is used to degrade the 250 MeV beam produced by our cyclotron down to 70 MeV for treatments. To reach such low energies, the momentum spread after the carbon degrader is about ±4.5%. However, due to the design of the beamline, a maximum momentum spread of ±1.3% can be transported through the ESS, and by using different positions of the slit, the momentum spread can be reduced down to ±0.1%.

The beam optics for the OPTIS2 beamline have been designed to transport the maximum acceptable emittance through the beamline (48 π mm mrad in the *X* plane and 100 π mm mrad in the *Y* plane) to maximize transmission. Ocular treatments, however, require a low momentum spread (±0.25%) to maximize the distal fall-off of the Bragg peak, as discussed above. This currently limits the dose rate that can be delivered to the patient to 15 Gy min^{-1} (total transmission, 0.27%) from the cyclotron to the isocentre, corresponding to treatment times of about 1 min. This is not ideal for treatments, as the patients need to keep their eyes open and focus on a reference point, and the eyelids are kept open by an external clip. This can be difficult for many patients (and makes the treatment of children almost impossible), resulting in frequent treatment interruptions, which also extends the treatment time.

To separate the OPTIS2 beamline from other beamlines in our facility (not shown in Fig. 3), we use the bend (D3–Q14–Q15–Q16–Q17–D4) that forms a small achromatic beamline similar to an ESS. As such, for our tests of momentum cooling, we inserted the wedge between quadrupoles Q15 and Q16 (Fig. 3). Supplementary Table 2 provides a comprehensive specification of the eye beamline, outlining its detailed characteristics.

For our experiment, we kept the slit open so that we could transport the beam with a momentum spread of ±1.3% up to the wedge, with the aim of reducing the momentum spread to less than ±0.3% using a polyethylene wedge (density, 0.94 cm^3) that was 4.00 cm high, 4.00 cm wide and with the maximum thickness of 0.38 cm. The geometry of the wedge was determined based on the momentum spread of the beam and the dispersion function at the location of the wedge. As a result of scattering in the wedge, the beam's emittance increased, leading to an emittance of approximately 94 π mm mrad in the *X* plane and 107 π mm mrad in the *Y* plane (this emittance was experimentally measured using two profile monitors after Q22). After the wedge, to keep the beam inside the beam pipe, we focus the beam in the *X* plane using quadrupole Q16. We also adjust the magnetic field of the dipole magnet D4 to compensate for the energy loss accrued in the wedge. Quadrupoles Q18–Q22 were used to achieve zero dispersion and double waist at the entrance of the OPTIS2 room. To measure the momentum spread of the beam, we measured the Bragg peak curve in water at the isocentre and deduced the momentum spread from the distal fall-off of the beam. By selecting the clinically used momentum spread (±0.25%) with a slit and transporting the beam up to the isocentre (that is, without the wedge inserted in the beamline), a distal fall-off (80–20%) of 0.91 mm was measured (Fig. 3b). When transporting a beam with a momentum spread of ±1.30% with the wedge in place, together with new beam optics to compensate for the resulting change in momentum spread and emittance, we measured a distal fall-off (80–20%) of 0.99 mm (Fig. 3c), corresponding to a substantially reduced momentum spread of ±0.27% at the entrance of the OPTIS2 treatment room. In this configuration, we measured a transmission of 0.5% (28.5 Gy min^{-1}) from the cyclotron to the entrance of the OPTIS2 treatment room, almost double the original 0.27% transmission of the clinical beamline when using slits. As the irradiation time is proportional to the beam current, this would correspond to treatment time reductions of a factor of 2 (60 s down to 30 s). Transmission could be further improved by redesigning the ESS (by using a smaller bending angle, that is, 15°) to transport the

https://doi.org/10.1038/s41567-023-02115-2

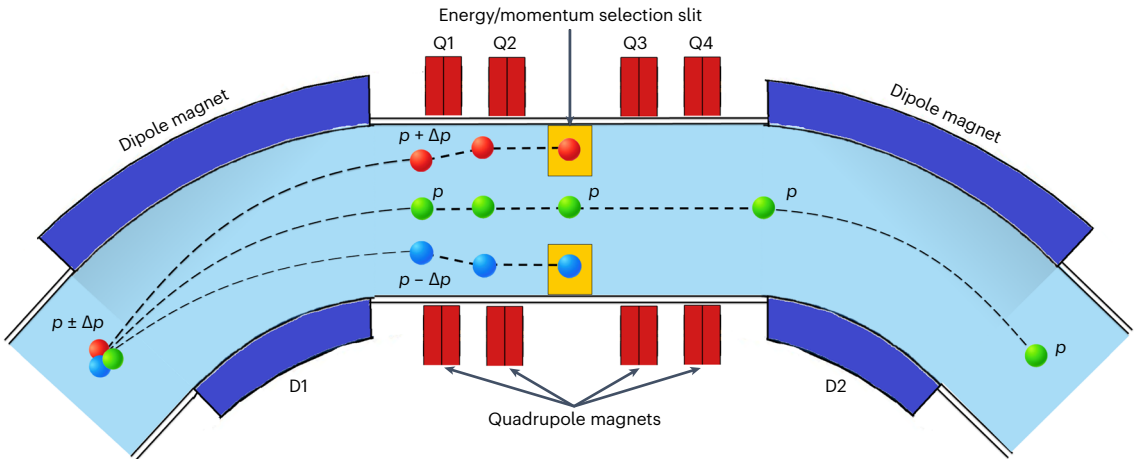

Fig. 1 | Layout of conventional ESS with a cross section in the bending plane. Q1–Q4 are quadrupole magnets. D1 and D2 are dipole magnets. Off-momentum particles are stopped by the energy/momentum selection slit made of copper. Here p represents the momentum of the particle and Δp represents the maximum momentum spread in the beam. The particle trajectories are defined based on the momentum of the particle.

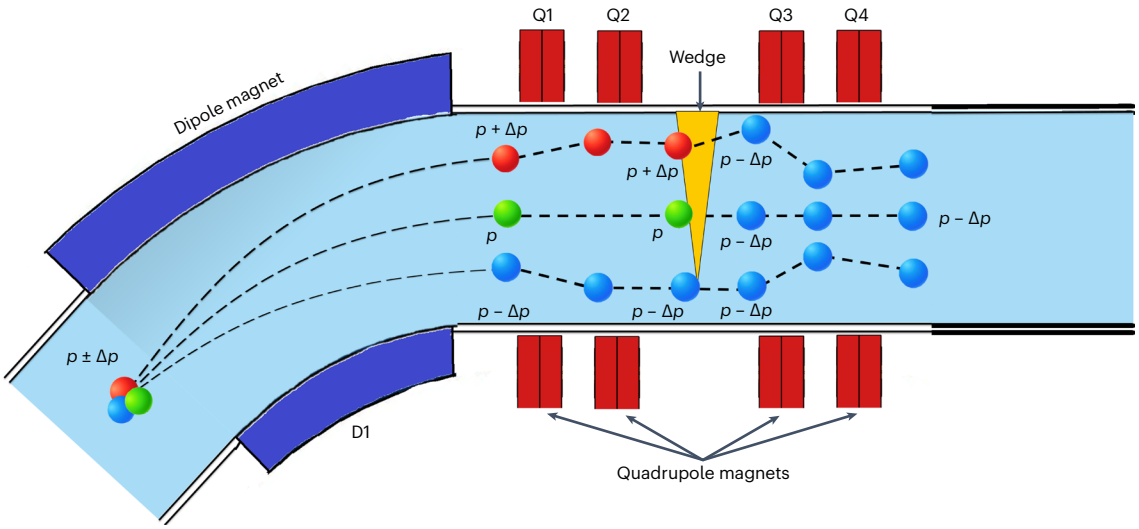

Fig. 2 | Layout of new ESS with momentum cooling with a cross section in the bending plane. Wedge is made of a low-Z material (that is, polyethylene or polymethylmethacrylate). Q1–Q4 are quadrupole magnets. D1 is a dipole magnet. Here p represents the momentum of the particle and Δp represents the maximum momentum spread in the beam. The particle trajectories are defined based on the momentum of the particle.

maximum momentum spread (±4.5% at 70 MeV). With this modification, we would expect a transmission of almost 7%, corresponding to a dose rate of about 390 Gy min^{-1} and treatment times of the order of 3 s, which could open the door to treat new patient groups (that is, young children) having ocular cancer with PT. Due to these encouraging results, we are currently preparing to implement this solution for clinical use in the OPTIS2 beamline.

Performance characteristics of PT facility with momentum cooling

Beam transport through a gantry-based treatment facility is more complicated than for a fixed beamline, and it is important to have the same emittance in both transverse planes at the entrance of the gantry to achieve gantry-angle-independent beam optics, transmission and beam size at the isocentre[8]. This can limit the achievable transmission. As such, we have also investigated the application of momentum cooling to the design of a compact PT gantry. A schematic of this, based on a commercial 250 MeV cyclotron with the maximum extracted beam current of 800 nA (ref. 19), is shown in Fig. 4. The first three quadrupoles (Q1–Q3) are used to focus the beam at the centre of an energy degrader (made of beryllium), which determines the energy within the clinically required range (70–230 MeV) and achieving the smallest increase in beam size. Asymmetrically shaped emittance selection collimators (already mounted on the gantry) are then used to select the maximum acceptable emittance for Q4 and Q5.

With this approach, two times higher emittance can be transported in the Y plane compared with the X plane (bending plane). This quadrupole pair then focuses the beam at the entrance of the new ESS (beamline made of D1–Q6–Q7–wedge), while the dipole magnet D1 (bending angle, 15°) is used to sweep the beam over the wedge in the dispersive focus. After the first bending magnet, we use the collimator to clean the beam tails (the collimator is not shown in Fig. 4). After this, quadrupoles Q6 and Q7 are used to achieve the smallest possible beam size (for a beam with zero momentum spread) in a dispersive plane at the location of the wedge. If made of polyethylene (density, 0.94 g cm^{-3}) and with its thickness modified depending on the energy of the beam, this reduces the momentum spread ($\Delta p/p$) of the beam. The beamline design following the wedge is then similar to PSI's Gantry

https://doi.org/10.1038/s41567-023-02115-2

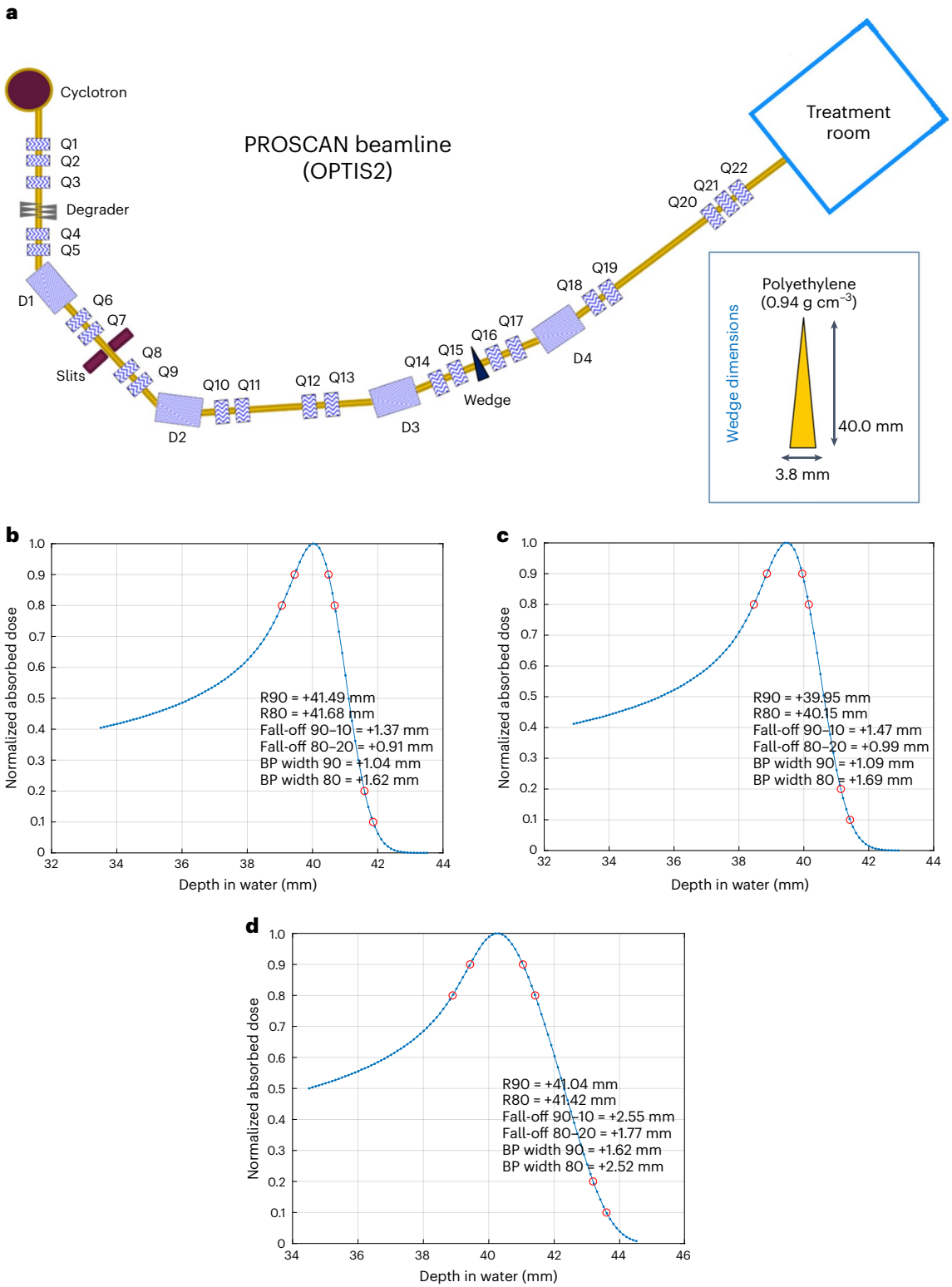

Fig. 3 | Eye beamline and Bragg peak shape exhibit variations in momentum spread. a, PROSCAN (OPTIS2) beamline used for ocular treatment. Q1–Q22 are quadrupole magnets and D1–D4 are dipole magnets. A wedge can be inserted between Q15 and Q16. **b**, Measured Bragg peak curve in water at isocentre transporting momentum spread of ±0.25% (using slit in ESS) and keeping the wedge outside the beamline. **c**, Measured Bragg peak curve in water at isocentre transporting momentum spread of ±1.3% and keeping the wedge inside the beamline. The momentum spread after the wedge is ±0.27%. **d**, Measured Bragg peak curve in water at isocentre transporting momentum spread of ±1.3% and keeping the wedge and slits outside the beamline. To define the distinct characteristics of the Bragg peak, the different ranges of proton beam in water are illustrated by the red circles in **b**–**d**. The terms R80 and R90 represent the proton range at which the Bragg peak (BP) fall-off reaches 80% and 90% of the normalized dose, respectively. Fall-off 90–10 and fall-off 80–20 represent BP fall-off distance between 90% and 10% as well as 80% and 20% of the normalized dose, respectively. BP width 90 and BP width 80 represent the Bragg peak width at 90% and 80% normalized absorbed dose, respectively.

https://doi.org/10.1038/s41567-023-02115-2

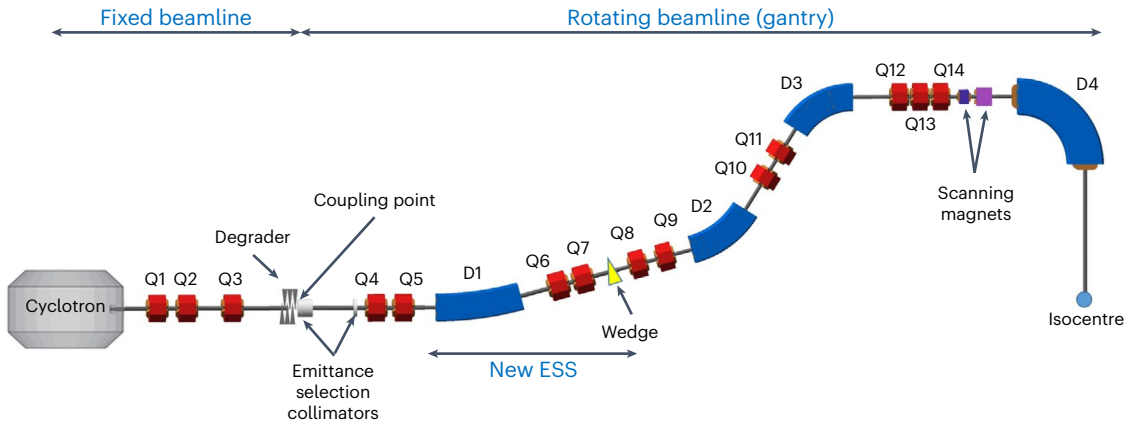

Fig. 4 | Layout of PT apparatus with momentum cooling capabilities (model from BDSIM). The cyclotron produces a beam with an energy of 250 MeV, which can be reduced by a degrader to a minimum of 70 MeV. The gantry beamline begins at the coupling point and offers a full 360° rotation. To reduce the momentum spread of the beam, an ESS with a variable-thickness wedge is employed. The thickness of the wedge can be adjusted based on the beam's energy. Scanning magnets are utilized to scan the beam and administer the dose to the entire tumour. Patient treatment takes place at the isocentre. Q1–Q14 are quadrupole magnets and D1–D4 are dipole magnets.

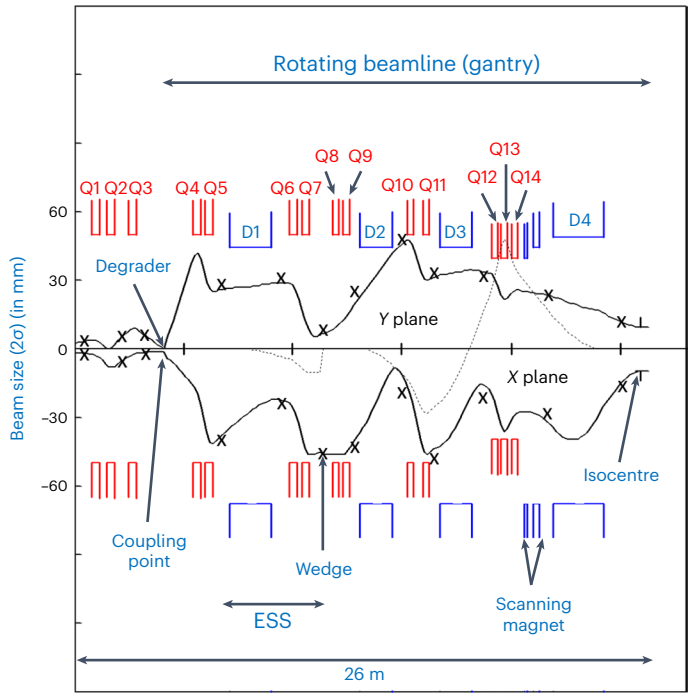

Fig. 5 | TRANSPORT beam envelope along the beamline. The new beam optics with a wedge transporting 48 π mm mrad in the *X* plane and 100 π mm mrad in the *Y* plane up to the wedge location. The beam envelope (Fig. 4) shows the beam size in 2σ values and the dispersion (dashed line) along the beamline (the lower half shows the beam envelope in the *X* plane (bending plane) and the upper half shows the envelope in the *Y* plane.). The x markers show the beam size from the BDSIM simulation along the beamline. Typically, the beam shape along the beamline follows a Gaussian distribution. During the beam-optics design phase, it is common practice to use 2σ (σ is the standard deviation of the distribution of sizes of the beam) values to effectively represent the beam envelope.

2 (ref. 20). Supplementary Table 1 provides a detailed specification of the full layout.

The beam optics for this layout have been designed using the matrix formalism code TRANSPORT[21]. The emittance selection collimators define the maximum acceptable emittance of 48 π mm mrad in the *X* plane and 100 π mm mrad with a beam envelope in the *Y* plane through the gantry (for the 70 MeV beam) (Fig. 5). In addition, the Monte Carlo simulation-based simulation code BDSIM[22], previously validated experimentally for our beamline[8,15], has been used to calculate the transmission of the different energy beams along such a beamline. For the lowest-energy beam to be transported (70 MeV), the wedge could be made of polyethylene (density, 0.94 g cm^{-3}) with dimensions of 8.00 cm height, 8.00 cm width and with a thickness of 1.13 cm. The required dimensions of the wedge for higher-energy beams are calculated based on the momentum spread of the beam after the energy degrader. The use of a wedge at the location of maximum dispersion, however, substantially increases the emittance of the beam in the bending plane. Therefore, to transport higher emittances in the *X* plane, the beam optics after the wedge have been designed such that we have a large beam size and low divergence in the first two quadrupoles (Q8 and Q9) after the wedge. In this way, the losses can be minimized after the wedge and the beam envelope is preserved inside the beam pipe downstream of the wedge location, thus achieving the maximum transmission following the approach proposed in our previous study[15].

Monte Carlo simulations indicate that the use of the wedge in the ESS could reduce the momentum spread of the 70 MeV beam from ±4.0% to ±0.6% and allowing for transmission of 10.0% from the cyclotron to the isocentre. This is almost a factor of 100 higher transmission than current state-of-the-art cyclotron-based facilities (transmissions of typically ~0.1%). This is due to three factors. First (1.7 times improvement), the use of a beryllium degrader decreases emittance compared with carbon and boron carbide degraders commonly used in PT facilities[7]. Second (6 times improvement), the use of asymmetric collimators after the degrader allows to maximized emittance and minimizes losses. Third and the main reason (~10 times improvement) is the use of momentum cooling, along with improved beam optics after the wedge. Increases in transmission are also predicted over all the transportable energies, with transmissions of 67% being predicted for a 230 MeV beam. These transmissions correspond to maximum currents at the isocentre of 80 nA for 70 MeV and 536 nA for 230 MeV beams, assuming 800 nA can be extracted from the cyclotron. Transmissions and maximum achievable beam currents at the isocentre for all the clinical energies are shown in Fig. 6a.

Along with the transmission/dose rate, however, it is also important to maintain a small beam size at the isocentre. In our simulations, we achieved beam sizes (σ) ranging from 4.0 mm (230 MeV beam) to 9.5 mm (70 MeV beam) (Fig. 6b), which are similar to some commercial

https://doi.org/10.1038/s41567-023-02115-2

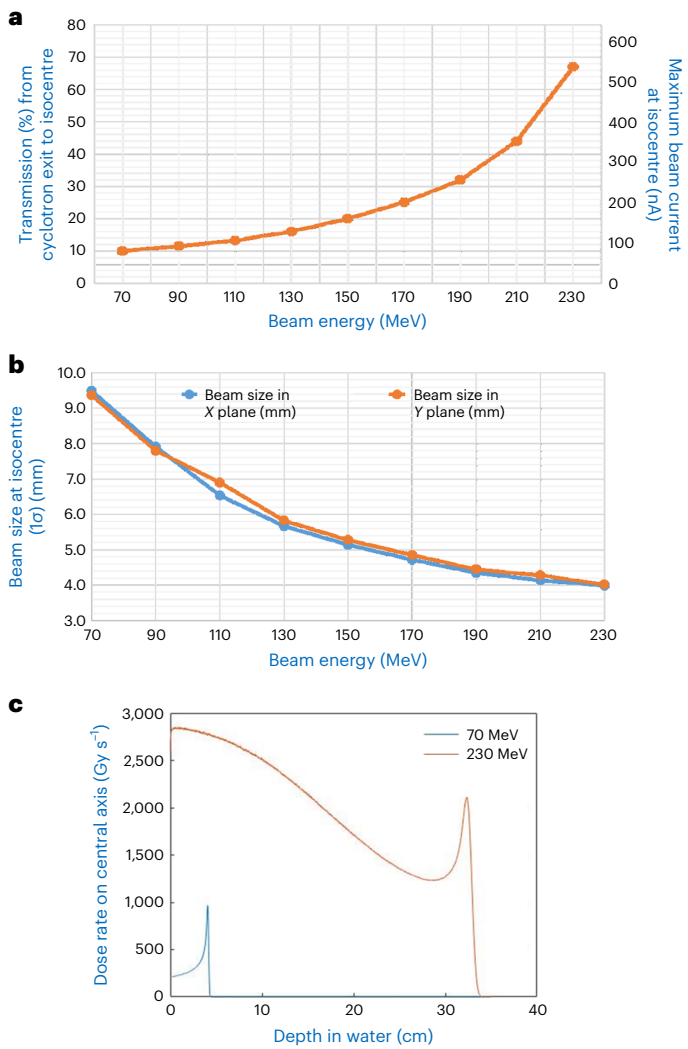

Fig. 6 | Performance characteristics of PT facility with momentum cooling. **a**, Simulation results for transmission (%) and the maximum achievable beam current (nA) (systematic uncertainty of ±2.5% and statistical uncertainty of ±1.6%) of different clinically used beam energies from cyclotron to the isocentre. **b**, Beam size at the isocentre for different energy beams (with an uncertainty of ±3%). In general, the treatment planning system defines the beam using a 1σ value (σ is the standard deviation of the distribution of sizes of the beam). Consequently, we utilize the 1σ value as the definition at the isocentre. **c**, Comparison of Bragg peak curves on the central axis for the 70 and 230 MeV beams. All the error bars represent the absolute minima and maxima. In **a** and **b**, the lines connecting two data points represent the approximate transmission values.

PT facilities (for example, IBA machines)[23,24]. This combination of ultrahigh beam current and relatively narrow beam sizes at the isocentre would provide the maximum dose rates of 952 and 2,105 Gy s^{-1} on the central axis of the Bragg peak (in water) for 70 and 230 MeV beams, respectively (Fig. 6c).

Practical realization and clinical relevance

We have experimentally demonstrated that the use of an ESS with a momentum cooling wedge, aimed at reducing the momentum/energy spread of the beam in a cyclotron-based PT facility, can achieve substantially higher transmission for low-energy beams. This straightforward yet elegant approach overcomes the limitations of a typically used ESS with slits, by slowing down the particles of higher momentum to match the speed of low-momentum particles of the beam. In the simulation, we have shown that with a gantry design incorporating this feature, we can achieve almost a factor of 100 higher transmissions for 70 MeV beams compared with conventional cyclotron-based facilities. In addition, as the gantry starts just after the degrader, the emittance at the entrance of the gantry is symmetric in both planes, resulting in gantry-angle-independent beam optics, transmission and beam size at the isocentre.

The concept could also be extended to cyclotron-based multiple-treatment-room facilities. Most of such facilities use a single ESS. To optimize transmissions, we propose to transport the maximum acceptable emittance through the beamline, which is different in both transverse planes. Additionally, the wedge-based ESS concept increases the emittance of the beam in the bending plane and we will, therefore, get different emittances at the entrance of the gantry, leading to gantry-angle-dependent beam optics and transmission. However, in previous work, it has been shown that scattering foils can efficiently equalize the emittances[25] in PT beamlines, and the use of such a foil between the new ESS and gantry entrance to match the emittance in both planes could be employed. Although increased emittance caused by the scattering foil would somewhat reduce the beam transmission through the gantry, the total transmission would still be substantially higher compared with conventional facilities.

One of the challenges of the proposed wedge system is that slightly different wedge thicknesses need to be used for each 10 MeV energy change. For this, a fast, stepped wheel with different, energy-specific wedges could be envisaged. Nevertheless, the extent to which the transmission increases varies depending on the specific facility, owing to variations in distances, apertures, materials and cyclotron energies. As such, and as a proof-of-principle study, we have modified IBA Proteus One type of single-room gantry design model[26] to add momentum cooling capabilities. With this design, in simulations, we also achieve nearly 3% transmission for a 70 MeV beam, which is almost a factor of 30 higher compared with the existing design.

Recently, the radiation therapy community has been exploring the potential of ultrahigh dose rates in cancer treatment[10]. Preclinical evidence suggests that such dose rates (>40 Gy s^{-1}) could substantially improve normal tissue sparing and maintaining high tumour control compared with conventional dose rates (~0.1 Gy s^{-1})[27]. Currently, FLASH dose rates can only be achieved using the highest beam energies (that is, those with the best transmissions through the beamline and gantry) in transmission (shoot-through) mode[28,29]. Unfortunately, this approach sacrifices the principal advantage of particle therapy, that is, the use of the Bragg peak to completely spare normal tissues distal to the tumour. As demonstrated in our simulation study, however, by using momentum cooling in the beamline, it is possible to achieve a dose rate of 952 and 2,105 Gy s^{-1} at the Bragg peak (in water) for the 70 and 230 MeV beams, respectively. When combined with the use of field-specific ridge filters[30–32], this will allow for Bragg-peak-based FLASH PT.

In addition, despite the substantial dosimetric advantages of pencil-beam-scanning[33,34] PT over conventional radiotherapy, challenges still remain to optimally treat mobile tumours, that is, tumours in the thorax and abdomen that are substantially affected by breathing motion[35–37], as well as worries over the substantial costs associated with the technique[38]. The use of momentum cooling could potentially help with both.

First, delivery uncertainties due to motion can be substantially reduced if patients can be treated within a single breath-hold. The ultrahigh dose rates that could be achievable using momentum cooling, in combination with methods for optimizing (minimizing) the number of pencil beams in pencil-beam-scanning PT[39,40], will allow for field deliveries well within a single breath-hold (<5 s)[11] even for the treatment of moving targets with increased patient comfort. Even two-field treatments could possibly be delivered within 20–25 s, which could also be achievable for patients using deep-inspiration breath-hold[41].

Such an approach has the potential to open new windows for treating different types of cancer with PT.

The second impact of high transmission may come in terms of investment cost reduction. For most PT facilities, based on the radiation protection requirement of the specific country, the shielding is designed based on the maximum achievable beam current at the highest energy of the beam. However, in current cyclotron-based PT facilities, due to the poor transmission for low-energy beams, it is required to extract a higher beam current (~800 nA) from the cyclotron. This led to thick concrete shielding around the facility and results in a substantial increase in investment cost. Due to higher transmission, the use of momentum cooling allows the users to limit the maximum beam current required from the cyclotron, as fast treatments (for example, single deep-inspiration breath-hold delivery) may already be possible with cyclotron currents as low as 50 nA. Therefore, the ESS with momentum cooling proposed here enables the development of highly compact (in terms of shielding) PT facilities, thus substantially reducing the size and cost of PT.

Online content

Any methods, additional references, Nature Portfolio reporting summaries, source data, extended data, supplementary information, acknowledgements, peer review information; details of author contributions and competing interests; and statements of data and code availability are available at https://doi.org/10.1038/s41567-023-02115-2.

References

1. Peeva, A. *Cyclotrons—What are They and Where Can you Find Them* https://www.iaea.org/newscenter/news/cyclotrons-what-are-they-and-where-can-you-find-them (2021).
2. Jermann, M. *Particle Therapy Facilities in Clinical Operation* https://www.ptcog.ch/index.php/facilities-in-operation (2022).
3. Lomax, A. J. et al. A treatment planning inter-comparison of proton and intensity modulated photon radiotherapy. *Radiother. Oncol.* **51**, 257–271 (1999).
4. Ladra, M. M. et al. A dosimetric comparison of proton and intensity modulated radiation therapy in pediatric rhabdomyosarcoma patients enrolled on a prospective phase II proton study. *Radiother. Oncol.* **113**, 77–83 (2014).
5. Eaton, B. R., MacDonald, S. M., Yock, T. I. & Tarbell, N. J. Secondary malignancy risk following proton radiation therapy. *Front. Oncol.* **5**, 261 (2015).
6. Gerbershagen, A. et al. Measurements and simulations of boron carbide as degrader material for proton therapy. *Phys. Med. Biol.* **61**, N337–N348 (2016).
7. Anferov, V. Energy degrader optimization for medical beam lines. *Nucl. Instrum. Methods Phys. Res. A* **496**, 222–227 (2003).
8. Maradia, V. et al. A new emittance selection system to maximize beam transmission for low-energy beams in cyclotron-based proton therapy facilities with gantry. *Med. Phys.* **48**, 7613–7622 (2021).
9. Chang, J. Y. et al. Consensus guidelines for implementing pencil-beam scanning proton therapy for thoracic malignancies on behalf of the PTCOG thoracic and lymphoma subcommittee. *Int. J. Radiat. Oncol. Biol. Phys.* **99**, 41–50 (2017).
10. Montay-Gruel, P. et al. Hypofractionated FLASH-RT as an effective treatment against glioblastoma that reduces neurocognitive side effects in mice. *Clin. Cancer Res.* **27**, 775–784 (2021).
11. Maradia, V. et al. Ultra-fast pencil beam scanning proton therapy for locally advanced non-small-cell lung cancers: field delivery within a single breath-hold. *Radiother. Oncol.* **174**, 23–29 (2022).
12. Neuffer, D. et al. A wedge absorber experiment at MICE. In *Proc. International Particle Accelerator Conference (IPAC'17)* 2888–2890 (JACoW, 2017).
13. Stratakis, D. Application of passive wedge absorbers for improving the performance of precision-science experiments. *Phys. Rev. Accel. Beams* **22**, 053501 (2019).
14. Bogomilov, M. et al. Demonstration of cooling by the Muon Ionization Cooling Experiment. *Nature* **578**, 53–59 (2020).
15. Maradia, V. et al. Increase of the transmission and emittance acceptance through a cyclotron-based proton therapy gantry. *Med. Phys.* **49**, 2183–2192 (2022).
16. Maradia, V. et al. A novel beam optics concept to maximize the transmission through cyclotron-based proton therapy gantries. In *Proc. 12th International Particle Accelerator Conference (IPAC 2021)* (eds Lin, L. et al.) 2477–2479 (JACoW, 2021).
17. Fleury, E. et al. Characterization of the HollandPTC proton therapy beamline dedicated to uveal melanoma treatment and an interinstitutional comparison. *Med. Phys.* **48**, 4506–4522 (2021).
18. van Goethem, M. J., van der Meer, R., Reist, H. W. & Schippers, J. M. Geant4 simulations of proton beam transport through a carbon or beryllium degrader and following a beam line. *Phys. Med. Biol.* **54**, 5831–5846 (2009).
19. Schippers, M. et al. Beam intensity stability of a 250 MeV SC cyclotron equipped with an internal cold-cathode ion source. In *Cyclotrons and Their Applications 2007, Eighteenth International Conference* 300–302 (2007).
20. Pedroni, E. et al. The PSI Gantry 2: a second generation proton scanning gantry. *Z. Med. Phys.* **14**, 25–34 (2004).
21. Brown, K. L., Carey, D. C., Iselin, C. & Rothacker, F. *TRANSPORT: A Computer Program for Designing Charged Particle Beam Transport Systems*. Report No. CERN-80-04 (CERN, 1983).
22. Nevay, L. J. et al. BDSIM: an accelerator tracking code with particle–matter interactions. *Comput. Phys. Commun.* **252**, 107200 (2020).
23. Almhagen, E., Boersma, D. J., Nyström, H. & Ahnesjö, A. A beam model for focused proton pencil beams. *Phys. Med.* **52**, 27–32 (2018).
24. Shamurailatpam, D. et al. Characterization and performance evaluation of the first-proton therapy facility in India. *J. Med. Phys.* **45**, 59–65 (2020).
25. Maradia, V. et al. Application of a scattering foil to increase beam transmission for cyclotron based proton therapy facilities. *Front. Phys.* **10**, 919787 (2022).
26. Tesse, R. *Quantitative Methods to Evaluate the Radioprotection and Shielding Activation Impacts of Industrial and Medical Applications using Particle Accelerators*. PhD thesis, Univ. Libre de Bruxelles (2018).
27. van de Water, S., Safai, S., Schippers, J. M., Weber, D. C. & Lomax, A. J. Towards FLASH proton therapy: the impact of treatment planning and machine characteristics on achievable dose rates. *Acta Oncol.* **58**, 1463–1469 (2019).
28. Jolly, S., Owen, H., Schippers, M. & Welsch, C. Technical challenges for FLASH proton therapy. *Phys. Med.* **78**, 71–82 (2020).
29. Nesteruk, K. P. et al. Commissioning of a clinical pencil beam scanning proton therapy unit for ultra-high dose rates (FLASH). *Med. Phys.* **48**, 4017–4026 (2021).
30. Kostjuchenko, V., Nichiporov, D. & Luckjashin, V. A compact ridge filter for spread out Bragg peak production in pulsed proton clinical beams. *Med. Phys.* **28**, 1427–1430 (2001).
31. Akagi, T. et al. Ridge filter design for proton therapy at Hyogo Ion Beam Medical Center. *Phys. Med. Biol.* **48**, N301–N312 (2003).
32. Sakae, T. et al. Multi-layer energy filter for realizing conformal irradiation in charged particle therapy. *Med. Phys.* **27**, 368–373 (2000).

33. Pedroni, E. et al. The 200-MeV proton therapy project at the Paul Scherrer Institute: conceptual design and practical realization. *Med. Phys.* **22**, 37–53 (1995).
34. Haberer, T., Becher, W., Schardt, D. & Kraft, G. Magnetic scanning system for heavy ion therapy. *Nucl. Instrum. Methods Phys. Res. A* **330**, 296–305 (1993).
35. Bert, C., Grözinger, S. O. & Rietzel, E. Quantification of interplay effects of scanned particle beams and moving targets. *Phys. Med. Biol.* **53**, 2253–2265 (2008).
36. Seco, J., Robertson, D., Trofimov, A. & Paganetti, H. Breathing interplay effects during proton beam scanning: simulation and statistical analysis. *Phys. Med. Biol.* **54**, N283–N294 (2009).
37. Phillips, M. H. et al. Effects of respiratory motion on dose uniformity with a charged particle scanning method. *Phys. Med. Biol.* **37**, 223–234 (1992).
38. Bortfeld, T. R. & Loeffler, J. S. Three ways to make proton therapy affordable. *Nature* **549**, 451–453 (2017).
39. van de Water, S. et al. Shortening delivery times for intensity-modulated proton therapy by reducing the number of proton spots: an experimental verification. *Phys. Med. Biol.* **65**, 095008 (2020).
40. Maradia, V. et al. Universal and dynamic ridge filter for pencil beam scanning particle therapy: a novel concept for ultra-fast treatment delivery. *Phys. Med. Biol.* **67**, 225005 (2022).
41. Emert, F. et al. Enhanced deep-inspiration breath hold superior to high-frequency percussive ventilation for respiratory motion mitigation: a physiology-driven, MRI-guided assessment toward optimized lung cancer treatment with proton therapy. *Front. Oncol.* **11**, 621350 (2021).

Methods

Beam-optics design and optimization

Matrix formalism code TRANSPORT[21] has been used to design the beam optics for our single-room gantry design. Since TRANSPORT cannot simulate the beam passing through the material, the beam optics were optimized independently for the following three sections of the beamline: (1) cyclotron exit to energy degrader, (2) exit of energy degrader to wedge location and (3) exit of the wedge to the isocentre; furthermore, we redefined the beam parameters at the transition points (exit of degrader and exit of wedge). For the first part, the beam optics are designed to focus the 250 MeV beam at the centre of the energy degrader to achieve a minimum increase in beam size after the degrader. At the exit of the degrader, the dispersion function is zero and we have a beam waist. At the start of the second part, we define beam parameters of 4 mm beam size and 12 mrad divergence in the X plane (48 π mm mrad emittances) and 4 mm beam size and 25 mrad divergence in the Y plane (100 π mm mrad emittances). For the beam with a momentum spread of zero, the beam optics were designed to achieve 2:1 imaging (in the bending plane) between the degrader exit and wedge location. This means that in the bending plane (in our case, the X plane), we will get a very small beam size of 2 mm at the wedge location. However, for low-energy beams, the momentum spread in the beam is about ±4%. Therefore, due to the dispersion introduced by dipole magnet D1, we get a large beam size of 45 mm at the wedge location with the proper distribution of momentum. However, there is no dispersion in the Y plane and here the beam size at the wedge location is about 7.5 mm with ~14 mrad divergence. When the beam passes through the wedge, we get almost similar beam momentum with a momentum spread of ±0.2% to ±0.6% depending on the energy of the beam. After the wedge, we get a minimum increase in emittance in the Y plane as the scattering contribution is smaller compared with the beam divergence at the entrance of the wedge. However, there will be a substantial increase in beam emittance after the wedge in the X plane depending on the energy of the beam. Therefore, the beam optics for the third part (wedge to isocentre) is separately designed for every 10 MeV beam from 70 to 230 MeV. Similar to the exit of the degrader, at the exit of the wedge, we have zero dispersion and beam waist. We designed the beam optics to achieve a 10 mm beam size (2σ) in a vacuum and achieving zero dispersion and double waist at the isocentre.

Monte Carlo simulations

TRANSPORT cannot calculate beam losses along the beamline. To calculate the transmission, momentum spread (after degrader and after wedge), dispersion function of the beam as well as the beam size at the isocentre and along the beamline, Monte Carlo simulations were conducted. These simulations utilized the BDSIM 1.4.1 Monte Carlo simulation toolkit. BDSIM is a powerful tool based on the Geant4 toolkit, capable of simulating diverse beamline components and magnets using Geant4 geometry. It provides accurate predictions of beam losses in particle accelerator/beamline components. The beamline settings were optimized with TRANSPORT, and the simulations were performed with the newly optimized beam optics. In our previous beam optics study, we built a model of PSI's PROSCAN beamline and Gantry 2 in BDSIM and validated it with the measurements[8]. For this study, we modified the PSI's Gantry 2 beamline and developed a model of a single-room gantry facility with momentum cooling in BDSIM. We used the same geometry as PSI's wedge degrader[42]. The calculations have been performed with the physics list based on the recommended modules for PT (G4StoppingPhysics, G4EmStandardPhysics_option4, G4HadronPhysicsQGSP_BIC_HP, G4HadronElasticPhysicsHP and G4EmStandardPhysicsWVI)[8]. Each simulation has been performed three times with 10 million initial particles to minimize statistical error. To experience the systematic uncertainty due to the choice of physics model in the transmission calculation, we repeated the simulations using two different physics models, namely, G4HadronPhysicsQGSP_BIC_AllHP and G4HadronPhysicsQBBC. Transmission differences between the two physics models were within ±2.5% (ref. 8).

Data availability

All data generated or analysed during this study are included in this Article and its Supplementary Information. Source data are provided with this paper.

Code availability

The code written for use in this study is available from the corresponding author upon reasonable request.

References

42. Oponowicz, E., Owen, H. L., Meer, D., Psoroulas, S. & Meer, D. Geometry optimisation of graphite energy degrader for proton therapy. *Phys. Med.* **76**, 227–235 (2020).

Acknowledgements

We express our gratitude to the sponsorship provided by PSI's CROSS funding scheme for supporting this work. We extend our thanks to D. Weber from the Center for Proton Therapy and M. Seidel from the Large Accelerator facility of PSI for their efforts in securing the funding for this project. Special appreciation is also conveyed to J. Hrbacek for his invaluable support during the measurements, as well as C. Baumgarten and M. Schippers for their insightful discussions. We are grateful for the assistance received from the cyclotron operation, technical support groups and radiation protection groups at PSI.

Author contributions

V.M. and S.P. designed and carried out the study and wrote the first version of the manuscript. R.D. prepared the experimental setup, and provided an analysis tool for the transmission measurement. V.M. and D.M. performed the measurement. S.P. is the primary investigator of the PSI CROSS grant that funds this research. S.P., D.M. and A.J.L. have significantly revised the manuscript at all stages and supervised the realization of this study in regular meetings. D.C.W. managed the funding and reviewed the article. All authors have read and approved the final manuscript.

Funding

Open access funding provided by Swiss Federal Institute of Technology Zurich.

Competing interests

A worldwide patent application (application no. EP22163081.7) has been submitted by V.M., D.M., S.P. and A.J.L. for the utilization of a wedge in PT to reduce the momentum spread of the beam. The application is currently under review. The other authors declare no competing interests.

Additional information

Supplementary information The online version contains supplementary material available at https://doi.org/10.1038/s41567-023-02115-2.

Correspondence and requests for materials should be addressed to Vivek Maradia.

Peer review information *Nature Physics* thanks Hsiao-Ming Lu, Stewart Boogert and the other, anonymous, reviewer(s) for their contribution to the peer review of this work.